Airflow Performance in Close Sided Vertical Channel

Ahmed Habeb *
Mathematic Department, Faculty of Science, Aljufra University, Houn, Libya
*Corresponding author: ahmed.habeb@ju.edu.ly

أداء تدفق الهواء في القناة العمودية ذات الجوانب المغلقة

احمد حبيب *
قسم الرياضيات، كلية العلوم، جامعة الجفرة، هون، ليبيا

Received: 15-04-2025; Accepted: 08-06-2025; Published: 19-06-2025

Abstract:
This paper reports on a natural convection experimental study conducted on a vertical test rig measuring 10 cm in height and 10 cm in width. The project was designed to collect temperatures and airflow velocities under different operating conditions, various channel depths and different heat inputs in order to obtain additional parameters required for analysis. The purpose and the main target of the project are to provide a clear picture of the flow behavior in this type of application. Extensive analysis was carried out to evaluate airflow rate, heat transfer coefficient and other related parameters. It was found that Nusselt number (Nu) is a function of the modified Rayleigh number (Ra*) and the aspect ratio (s/H). In addition, the Reynolds number Re(s) is a function of (Ra*) and (s/H). Dimensionless correlations between Nu, Re and Ra* were derived. Moreover, previous theoretical studies suggested that the flow rate should be proportional to the cube root of the heat input, while earlier experimental results indicate a higher exponent. However, the current experimental results suggest a value in between; the flow rate is demonstrated to be dependent on the aspect ratio, with a proportionality of approximately 0.66.

Keywords: Airflow Performance, Natural Convection, Vertical Channels.

الملخص:
تقدم هذه الورقة دراسة تجريبية حول الحمل الحراري الطبيعي تم إجراؤها على جهاز اختبار رأسي يبلغ ارتفاعه 10 سم وعرضه 10 سم. تم تصميم المشروع لجمع بيانات لدرجات الحرارة وسرعات تدفق الهواء تحت ظروف تشغيل مختلفة، أعماق قنوات متفاوتة ومدخلات حرارية مختلفة، بهدف الحصول على مقادير إضافية لازمة للتحاليل. الهدف الرئيسي من المشروع هو تقديم صورة واضحة لسلوك التدفق في هذا النوع من التطبيقات. تم إجراء تحليل موسع لتقييم معدل تدفق الهواء، ومعامل انتقال الحرارة، ومقادير أخرى ذات الصلة بالموضوع. قد تبين أن عدد نسلت (*Nu*) هو دالة لعدد رايلي المعدل (*Ra**) ونسبة الأبعاد (*s/H*). بالإضافة إلى ذلك، فإن عدد رينولدز (*Re(s*) هو دالة لـ (*Ra**) و(*s/H*). تم اشتقاق علاقات لا بعدية بين *Nu* و*Re* و*Ra**. علاوة على ذلك، أشارت الدراسات النظرية السابقة إلى أن معدل التدفق يجب أن يكون متناسبًا مع الجذر التكعيبي لمقدار الحرارة الداخلة، في حين أظهرت النتائج التجريبية السابقة قيمة أسية أعلى. ومع ذلك، تشير النتائج التجريبية الحالية إلى قيمة متوسطة؛ حيث تبيّن أن معدل التدفق يعتمد على نسبة الأبعاد، مع تناسب يقارب 0.66.

الكلمات المفتاحية: أداء تدفق الهواء، الحمل الحراري الطبيعي، القنوات الرأسية.

1. Introduction:

Heat transfer via natural convection is a passive process occurring in various applications due to temperature differences within the working fluid. This area of science has attracted researchers because fluid motion does not require any type of external mechanical assistance such as a fan or blower. Due to heat transfer exchange between the hot surface and the working fluid, there would be several thermal and physical relative aspects required to be investigated and analyzed. This would certainly lead to identifying, for example, flow regime, velocity/flow rate, and rate of heat transfer ... etc. This process is complex and highly dependent on geometry and other factors. Variations can include single-plate surfaces or vertical channels between two plates, open-sided or closed-sided channels, under either a uniform heat flux (UHF) or a uniform wall temperature (UWT). There are a wide range of studies that have been of interest and focused on by scientist. One example is the natural convection airflow over a single vertical plate, which is found in electrical applications, e.g. cooling fins. There have been numerous studies that addressed this phenomenon both theoretically and experimentally, deriving significant correlations relative to characterizing heat transfer rate and flow regimes [1-4]. Another example where natural convection flow is found in passive solar heating systems whose channel heights are usually more than 1 m, such as Trombe wall and thermosyphoing air panels [5-6]. Since the invention of the Trombe wall, there have been several series of theoretical and experimental works focused on heat transfer and airflow behaviour within UHF channels. For instance, extensive numerical studies were conducted on laminar and turbulence under the UHF heating mode simulating passive solar heaters [7-9]. In contrast, others [10-17] derived experimental correlations and obtained important findings based on indoor and outdoor experimental data that characterized airflow and heat transfer in UHF vertical channels larger than 1 m in height. The last

example is where natural convection typically occurs within smaller scale channels, similar to those found in electronic equipment. Since the early and pioneering work of Elenbass [18], extensive investigations have focused on buoyancy-driven convection between vertical plates. Following his work, several studies were performed on water and air as the working fluid under UWT heating mode. For example, experimental data were collected and correlations were derived for various channel aspect ratios (s/H) and plate inclination (ϴ) to explore the effect of inclination angle and the aspect ratio on the heat transfer behavior [19-24]. Finally, turbulent natural convection airflow between two small vertical plates, for symmetrically and asymmetrically heated channels, was experimentally investigated [25-26] to study the flow at both sides of the channel. Velocity profiles were tracked along both surfaces and reverse flow was detected at the cold surface.
This paper is an extension of the previous work of the author [27]. The current experimental work and the outcome of data analysis aimed at characterizing, in depth, the performance of heat transfer and airflow within an open-ended vertical small-scale channel (0.1 m x 0.1 m). The model was designed to accommodate various UHF heating inputs and different channel depths. The objective of this study is to explore how variations of heat inputs and channel depths influence the airflow and heat transfer behavior within the channel. The UHF mode is based on a constant heat flux added to the system. Therefore, Sparrow and Gregg [2] defined the modified Grashof number formula, for the UHF case, as follows:

$$\text{UHF heating mode Configuration:}\quad Gr^{*}=Gr(H)Nu(H) \Rightarrow Ra^{*}= Gr^{*}.\,Pr \;=\frac{g\,\beta\,q_c\,H^4}{\upsilon^2} \qquad (1)$$

UHF heating mode applications have not been explored enough in terms of example, heat transfer rate, flow rate and flow regime. The heat transfer rate and flow rate in terms of airflow velocity and flow rate will be extensively studied here and correlations will be derived. However, classifying the flow regime along this type of channel would be possibly looking at it in the future.

2. Experimental Set-up:

The experimental model configuration, Figure 1, consisted of a vertical channel open on the top, bottom, and closed on both sides. The channel measured 10 cm in height (H) and 10 cm in width (W) (heated plate area 0.01 m²). The channel depth was adjustable to three sizes (45, 55 and 65 mm). The hot plate was uniformly heated using electrical resistance, with four different power settings: 5, 10, 15, and 20 W. The opposite plate was constructed from a 2 mm thick aluminium sheet, positioned vertically opposite and parallel to the heated plate, and attached to a 10 mm MDF (Medium-Density Fibreboard) to minimize thermal losses. The sides of the channel were secured with hardwood pieces that matched the required depth. Type T copper-constantan thermocouples, each 0.2 mm in diameter, were installed to measure temperatures at the inlet, outlet, heated wall, plate, and the opposite wall, as shown in Figure 1. The thermocouples are located in the air stream and centered within lightweight silvered radiation shields made from thin plastic pipes, each approximately 20 mm long. These shields were specifically designed to minimize any influence on temperature readings within the channel. An additional separate thermocouple was used to monitor ambient temperature.

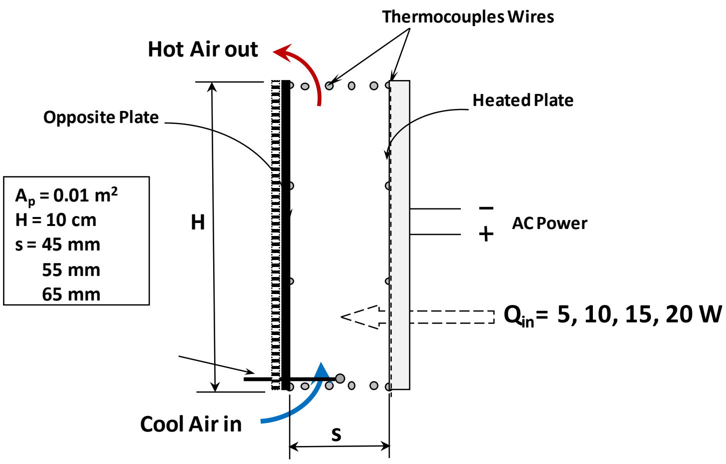

Figure 1: Schematic Diagram of the Experimental set-up (not to scale).

3. Experimental Procedure:

Prior to initiating the experiment and to ensure accurate results, all thermocouples were calibrated at the freezing and boiling points. The standard deviation of the calibration results at a 95% confidence level generally varied by ±0.5°C, while airflow measurements showed fluctuations of up to ±0.8°C. The hot plate had a standard deviation of ±1.2°C, whereas the opposite wall showed a standard deviation of ±0.9°C. Propagation rules were used to calculate the uncertainty values of all calculated parameters used in the project. The channel depths tested were 45 mm, 55 mm, and 65 mm, with three heat inputs; 5 W,10 W, 15 W and 20 W. Each test run was launched from a cold state (ambient temperature) and was left for a minimum of 2.5 hours to allow the system to reach a steady state. After each run, the system was allowed to cool overnight to ensure that the next run would begin at ambient temperature. Previous researchers have faced challenges in measuring airflow due to air leakage. To address this, a smoke test was conducted at the beginning of the experiment to ensure that no air was escaping from the test rig. This test was performed after the system had been heating for approximately 2.5 hours, and smoke was then introduced at the channel entrance while the exit vent was completely sealed. The results confirmed that there was no air leakage escaping outside the test rig. Air velocity was measured using a sensitive hot-bead anemometer model TA-5 manufactured by Airflow company. The anemometer was placed at the bottom of the channel to ensure consistent airflow velocity. The device provided an analog voltage output that could be recorded by the data logger. The accuracy of the device was calibrated at BSRIA Instrument Solutions, where it was determined to be ±(2% ±0.01m/s).

4. Results and Data Reduction:

4.1 Transient Response:

It is important to establish the time it takes the system for a given heat input to reach a steady state. The transient temperature and velocity data are closely aligned with an exponential model of the form:

$$y = y_o\,(1 - \exp(-k't)) \qquad (2)$$

The asymptote y_o from this model was used as the steady-state value for subsequent calculations. A proprietary curve-fitting software package, SigmaPlot, was employed to fit the data to the required exponential curve. From this curve, time constants (1/ k′) can be determined, as illustrated in Figure 2. The time constants (1/k′) for the overall system ranged from 30 to 70 minutes. For air in the channel, the typical time constant was approximately 60 minutes, while for the plate and cover, it was around 45 minutes.

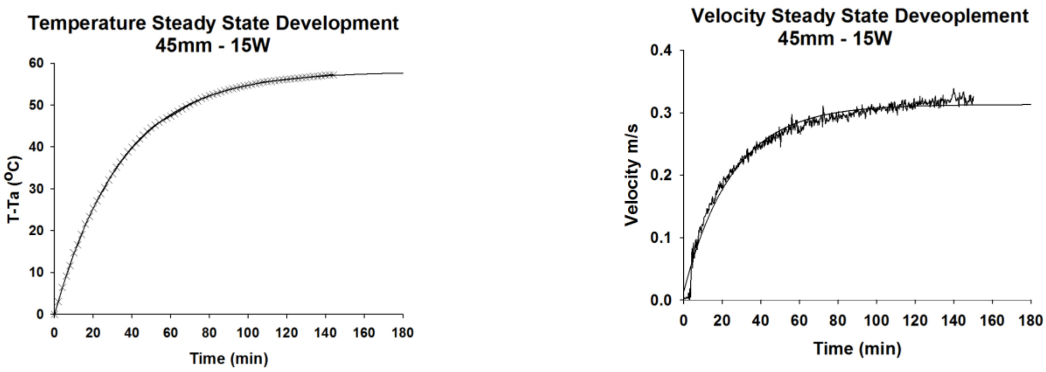

Figure 2: Typical Development of Airflow Temperature Velocity Development against Time

This indicates that the plate and cover reach a steady state before the airflow does. No consistent trends were observed for time constants in relation to heat input and channel depth. No further analysis currently has been conducted on the transient state, since the present study is focusing only on the steady state.

4.2 Flow Profiles:

The steady-state velocity data gives an indication of the airflow behaviour and flow development in the channel under the different operating conditions. The following measurements were taken when the system reached the steady state (after about two and a half-hour operation). The velocity meter probe was placed at the middle of the channel frame and readings of velocity were taken at specific intervals across the channel depth. The interval varied according to the depth of the channel. At each location, thirty readings were taken at five-second intervals in order to calculate the mean velocity at each measured point. The procedure was repeated until the whole channel gap was covered, at both the entrance and the exit. Figures 3a-c show the velocity profiles at the bottom of the channel for all the tested cases. The graphs clearly indicate that the velocities seem to be flat across most of the channel gap, which is expected as the flow enters the channel at an ambient condition (Ta and Pa), and were forced to be zero at both walls due to surface effect. The measurement elevation point of the velocity probe was not exactly at the edge of the entrance vent and was about 0.5cm inside the channel due to the test-rig construction frame. Figures 3d-f show the velocity profiles at the top of the channel also for all cases.

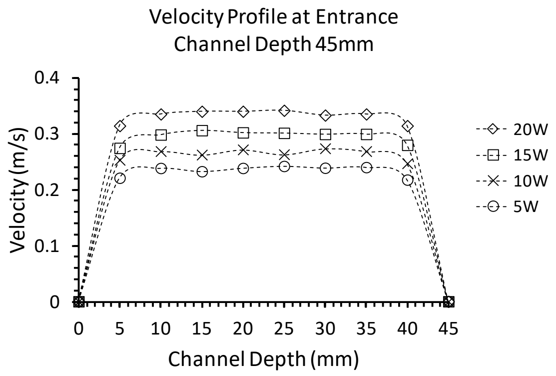

(a) **Entrance (45mm)**

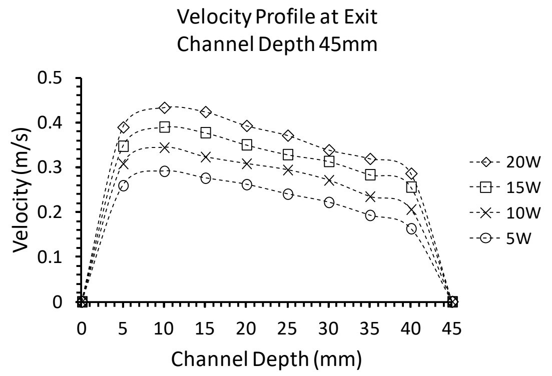

(d) **Exit (45mm)**

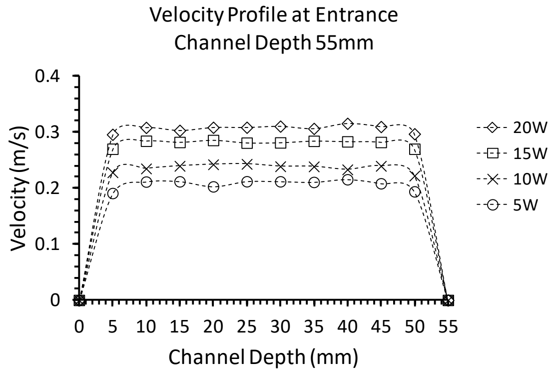

(b) **Entrance (55mm)**

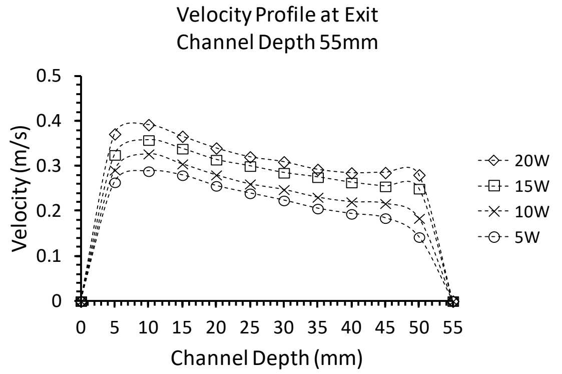

(e) **Exit (55mm)**

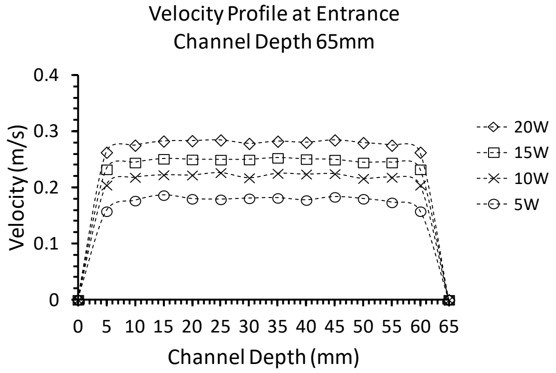

(c) **Entrance (65mm)**

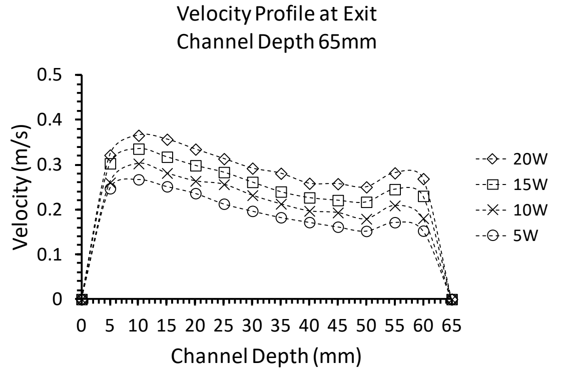

(f) **Exit (65mm)**

Figure 3: Velocity Profiles at the Entrance and the Exit of the Channel

It can be clearly noticed that the velocity is higher at the heated plate, and falls steadily towards the opposite wall, which is cooler (and boundary layers can be seen developing at both surfaces as the channel depth and heat input increase. This agrees qualitatively with observations made by [14]. However, it is clear that at no place does the velocity fall to zero, or even reverse flow occur [25-26] except at the two walls, which is normal due to wall shear force.

4.3 Mass Flow Rate and Heat Transfer Coefficient

As stated already, the air velocity profile across the channel was recorded at the bottom after a steady state had been achieved. The velocity profile was relatively flat, as expected near the inlet region, prior to the full development of the hydraulic boundary layers along the channel. To calculate the mass flow rate, the velocity at the bottom was taken as the bulk or average velocity (u_i). Thus, the mass flow rate ($\dot{m}$) was determined by the following formula [28]:

$$\dot{m} = \rho_i \, A_C \, \bar{u}_i \qquad (3)$$

The values of the calculated mass flow rate (Table 1) increase, as expected, with a wider channel depth (possibly due to reduction of friction forces) and higher heat input (could be due to higher temperature differences and buoyancy effects). The typical flow rate ranged from 0.0013 kg/s (at 45 mm, 5 W input) to 0.0022 kg/s (at 65 mm, 20 W input) agreed qualitatively, for instance, with [10].

Table 1: Mass Flow Rate based on Entrance Condition (kg/s)**.**

	5W	**10W**	**15W**	**20W**
45mm	0.0013	0.0014	0.0016	0.0018
55mm	0.0014	0.0016	0.0018	0.0020
65mm	0.0015	0.0017	0.0020	0.0022

Bouchair [11] discovered that for channel widths exceeding 300-500 mm (within aspect ratios of 0.2–0.3), the mass flow rate decreases as channel width increases. A numerical analysis performed by [7] within this range suggests an asymptotic straight line beyond an aspect ratio of 0.3, rather than a decline.

The average heat transfer coefficient ($\bar{h}$) is always lower in natural convection than in force convection due to the rate of heat transfer between the heat plate and the airflow. The heat transfer coefficient is calculated as follows [28]:

$$Q_c = \dot{m}\, c_p\, (T_o - T_i) \tag{4}$$

$$\bar{h} = \frac{Q_c}{A_p\,(T_p - T_m)} \tag{5}$$

Table 2 shows the values of the calculated heat transfer coefficient. It is clear that it decreases as the channel depth increases and increases as the heat input increases.

Table 2: Average Heat Transfer Coefficient (W/m^{2}K)**.**

	5W	**10W**	**15W**	**20W**
45mm	17.6	20.4	25.4	30.8
55mm	14.3	17.8	23.2	28.5
65mm	11.8	16.3	22.0	27.0

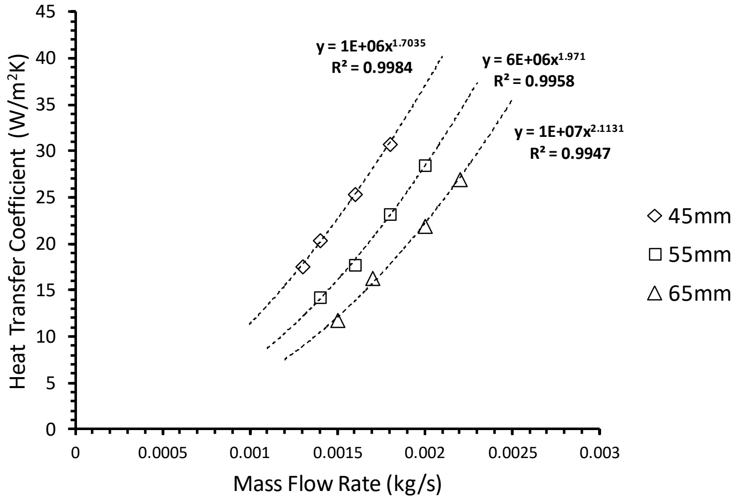

Figure 4: Heat Transfer Coefficient and Mass Flow Rate.

According to equations 3, 4 and 5, there is an indirect relationship between heat transfer coefficients ($\bar{h}$) and the mass flow rate ($\dot{m}$). The former is directly related to temperature differences between the heated plate, the adjacent fluid, physical properties of the fluid and the geometry, whereas the latter is mainly dependent on temperature differences because the increase in temperature differences and the increases in density difference result in an increase in bouncy force. Thus, the relationship between these two parameters cannot be linear because they both rely on similar factors. Figure 4 illustrates that the mass flow rate increases as the average heat-transfer coefficient increases for the same channel depth and various heat inputs with probably an exponential relationship as shown above each curve.

5. Dimensionless Correlations:

In order to complete the analysis and clarify the whole picture of the performance of the airflow due to natural convection in the vertical channel under the UHF mode, dimensionless correlations were developed between dimensionless groups and derived here. Nusselt numbers based on channel depth and height (Nu(s) and Nu(H)), modified Rayleigh number (Ra^*) and Reynolds number (Re(s)) are all correlated. This would allow the results to be extended more easily to correlate dimensionless equations and compared them with results from previous studies found in the literature. Nu(s) and Nu(H) are mainly based on heat transfer coefficient ($\bar{h}$) and are characterized by length (s or H), which can be obtained as follows [28]:

$$Nu(s) = \frac{\bar{h}\, s}{k_m} \tag{6}$$

$$Nu(H) = \frac{\bar{h}\, H}{k_m} \tag{7}$$

In addition, the Reynolds number, Re(s), is typically utilized in forced convection flow applications, but in this case, it is employed to describe the velocity or the flow rate of the airflow inside the channel, since there is no other dimensionless number playing the role. Re(s) is based on the channel depth (s) and determined as follows [28]:

$$Re(s) = \frac{\bar{u}_i\, s}{\nu_m} \tag{8}$$

This technique has been employed by other researchers, such as [10] and [15]. To establish correlations with other dimensionless groups, the Rayleigh number, Ra^*, is used for the Uniform Heat Flux problem [2], where temperatures of the surfaces and the airflow are unknown. This can be regarded as a dimensionless expression of heat input and takes the form of equation 1.

5.1 Dimensionless Numbers Variations:

The calculated dimensionless numbers, Nu(s), Nu(H), Ra^* and Re(s), were studied in terms of their variation with both convective heat transfer (Q_c) and aspect ratio (s/H), so that the effects of these parameters can be determined and correlations would be derived. Figures 4a through 4d show variations of Nu(s), Nu(H), Re(s) and Ra^* along with convective heat transfer (Q_c) and aspect ratio (s/H) . The suggested basic mathematical formula applied here is:

$$y = a\, x^b \tag{9}$$

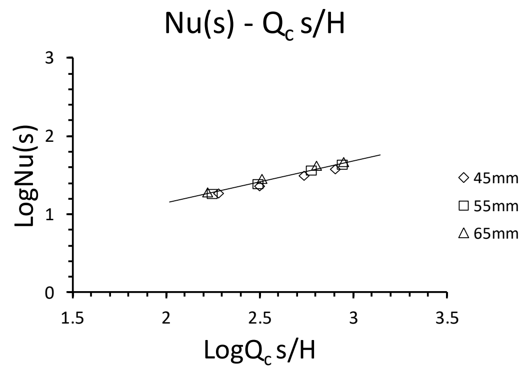

(a): Nu(s) against Q_c s/H

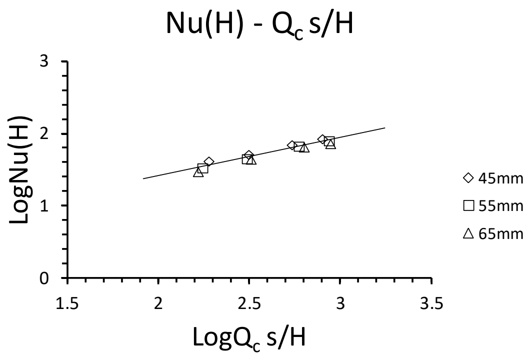

(b): Nu(H) against Q_c s/H

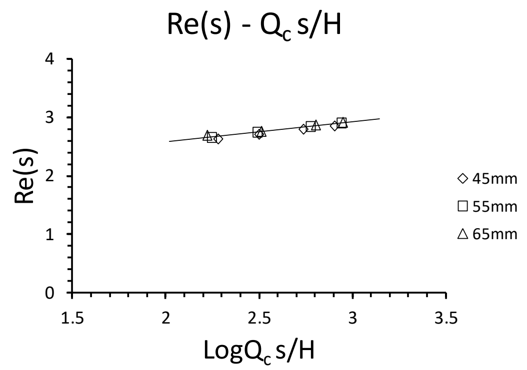

(c): Re(s) against Q_c s/H

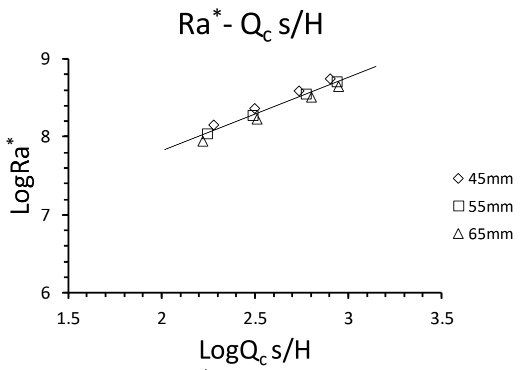

(d): Ra^* against Q_c s/H

Figure 5: Variations Dimensionless Number with Convective Heat Transfer and Aspect Ratio**.**

Figures 5a to 5d show the variation of Nu(s), Nu(H), Re(s) and Ra^* against Q_c s/H. It can be generally stated that all numbers increase as the Q_c s/H increases but no clear indication in the case of Nu(s) and Re(s) as both increase with channel depth (s) because they are both based on channel depth (s). All figures show very good linear relationships with good statistical regression analysis outcomes such as slandered errors (S. E) and correlation coefficient (R^2).

Correlated outcomes equations are listed below:

$$\mathrm{Nu(s)} = 1.164\,(Q_c\ \ s/H)^{0.538} \tag{10}$$

[S.E = 0.0349/R^2 = 0.95]

$$\mathrm{Nu(H)} = 2.224\,(Q_c\ \ s/H)^{0.531} \tag{11}$$

[S.E = 0.0405/R^2 = 0.94]

$$\mathrm{Re(s)} = 78.07\,(Q_c\ \ s/H)^{0.341} \tag{12}$$

[S.E = 0.0271/R^2 = 0.93]

$$Ra^* = 8 \times 10^5 (Q_c\ \ s/H)^{0.954} \tag{13}$$

[S.E = 0.0654/R^2 = 0.95]

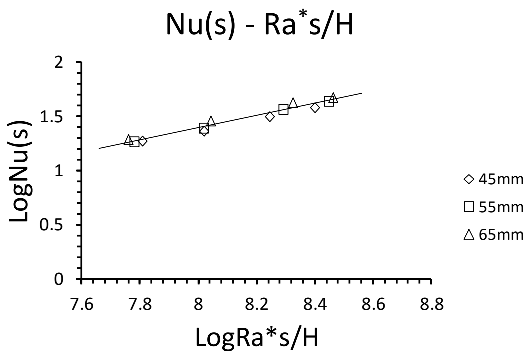

(a) Nu(s) against Ra(s/H)

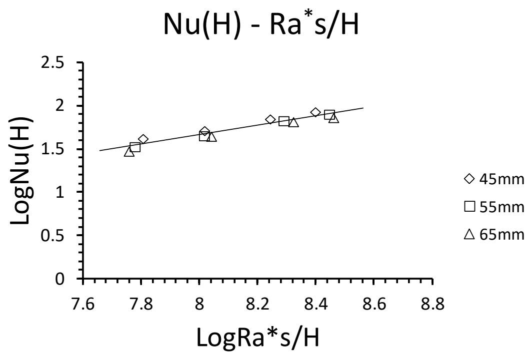

(b) Nu(H) against Ra^*(s/H)

Figure 6: Variation of Nu with Ra s/H.

5.2 Dimensionless Number Correlations:

Experimental data were developed to derive valid experimental correlations applicable to determining, for example, dimensionless heat transfer coefficient and flow rate. Derivations were further made to include the relationships between several dimensionless numbers, e.g. Nu, Re(s), and Ra^*. The least squares method and multiple regression analysis were used to evaluate the experimental constants throughout the derivation operation. Figures 6a and 6b show Nu(s) and Nu(H) being correlated against Ra^*s/H. It is clear that Nu(s) and Nu(H) increase as Ra^*s/H increases. Dimensionless equations for Nu(s) and Nu(H) along with their detailed statistical parameters results produced by SigmaPlot software give the following:

$$\mathrm{Nu(s)} = 0.0008\,(Ra^*\ \ s/H)^{0.563} \tag{14}$$

Statistical results show that: R^2= 0.97; mean percentage error of the data from the calculated regression line: 3.1%; a constant = 0.0008: standard error: 0.2955 (t-ratio: -10.51); index for Ras/H 0.563: standard error: 0.0363 (t-ratio: 15.51).

$$\mathrm{Nu(H)} = 0.0018\,(Ra^*\ \ s/H)^{0.551} \tag{15}$$

Statistical results show that: R^2= 0.90; mean percentage error of the data from the calculated regression line: 4%; a constant = 0.0018: standard error: 0.4087 (t-ratio: -6.71); index for Ras/H 0.55: standard error: 0.0502 (t-ratio: 10.96).

Figure 7 shows Re(s), as an indicator of airflow, being plotted against Ra^*s/H. Trends are clearly visible: Re(s) increases as Ra^*s/H. Standard multiple regression techniques can be used to quantify the dependency of flow rate on convective heat and aspect ratio. The dimensionless equation for Re(s) as a function of Ra^*s/H along with the detailed statistical parameters results produced by SigmaPlot software also gives the following:

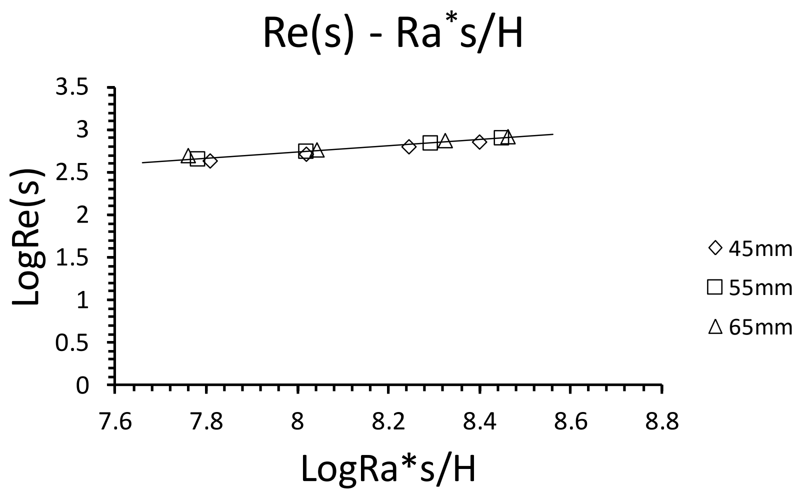

Figure 7: Variation of Re(s) with Ra s/H**.**

$$\mathrm{Re(s)} = 0.7602\ (\mathrm{Ra}^*\ s/H)^{0.357} \qquad (16)$$

Statistical results show that: R^2= 0.94; mean percentage error of the data from the calculated regression line: 3.2%; a constant = 0.7602: standard error: 0.2351 (t-ratio: -0.51); index for Ras/H = 0.357: standard error: 0.0289 (t-ratio: 12.35).

Another important outcome is that a theory based on a lumped-parameter model of buoyancy-driven airflow in a vertical channel suggests that flow rate is proportional to the cube root of the heat input (see, for example, Sandberg and Moshfegh [17].

$$\dot{m} \propto q_{in}^{\ 1/3} \qquad (17)$$

If the mathematical form is assumed to be:

$$\mathrm{Re(s)} = a\ (\mathrm{Ra}^*)^b.(s/H)^c \qquad (18)$$

In order to test the validity of this relationship, the exponent b in equation 18 was set to ⅓ and the data from the present study were plotted as:

$$\mathrm{Re(s)}.(\mathrm{Ra}^*)^{-1/3} = a.(s/H)^c \qquad (19)$$

The results are presented in Figure 8. The data points show little scatter, and therefore the lumped-parameter model can be regarded as a good representation. For all sets of data, the dependency of flow rate on the depth-to-height aspect ratio (s/H) is close to 0.66:

$$\dot{m} \propto (s/H)^{0.66} \qquad (20)$$

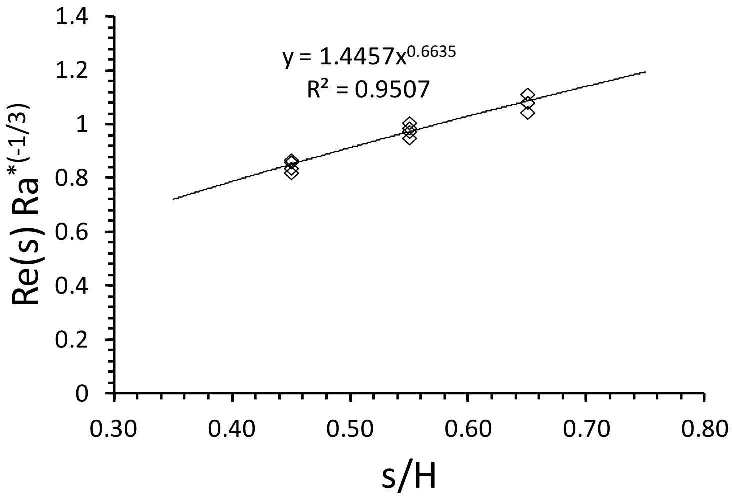

Figure 8: Flow Rate Dependence on Aspect Ratio**.**

Note that all the above-derived correlations are subject to the limits of the data, as follows:

$$0.45 \le s/H \le 0.65$$
$$5W \le Q_{in} \le 20W$$
$$1.09 \times 10^8 \le Ra^* \le 5.57 \times 10^8$$

7. Discussion:

The current empirical study was conducted under a lab condition on a small vertical closed sided channel (duct). At a thermal steady state condition, various UHF heating values and different aspect ratio (s/H) were tested to characterize the thermal and the hydraulic performance of the airflow in resembling channels. Although, natural convection studies in literature are rich of important publications, experimental woks under the UHF heating configuration on open-ended vertical channels are unexpectedly few. This makes it challenge to compare, discuss and validate the current study with previous published data. The analysis of the current collected experimental data was initially introduced the velocity profiles for all heat inputs (Q_{in}) and aspect ratio (s/H). The development stages of the velocity profiles along the channels are similar for the two types of the heating modes as the development generally occurs when both surfaces gains heat either symmetrically or asymmetrically. Velocity profiles in Figure 3 illustrate their development along the channel, which are commonly seen in similar natural convection studies. The purpose of obtaining the profiles is to draw the development stages of the hydraulic boundary layer of the flow along the channel and detect any disruption of flow that may occur, for example; reverse flow or recirculation, etc [14]. The profiles are almost flat at channel inlet (see figures 3a, b and c) where the flow enters the channel at the ambient temperature and ambient pressure (no heat exchange between the fluid and the walls yet). Similar qualitative observations were made, for example by, [14, 16, 29, 30, and 31]. However, profiles at the exit of channel were influences by the values of hating provided to the flow and the size of the channel depth. Figures 3d, 3e and 3f show the flow develops downstream and establishes two peaks at the heated surface and the opposite wall. Only one peak, at the heated surface, can be seen where the channel depth is narrow (Figure 3d) and the two peaks become clearly visible at both surfaces, particularly at the highest heat inputs and a wider channel depth (Figure 3f). [14, 16, 29, 30, and 31] achieved similar qualitative profiles, but some of them detected a reverse flow [25] and recirculation/eddies [14]. The mass flow and the calculated heat transfer coefficient were also obtained. Although they are both found to be a function of heat input (Q_{in}) and aspect ratio (s/H) (see Table 1 and 2), it was found that they both have no direct relationship. However, their relationship was found to be independently exponential to individual exponents depending on s/H and Q_{in} (see figure 4). The correlations of airflow under UHF heating mode are rare and the only two encountered publications in the literature are for small ducts were Vliet and Ross [4] for a heated surfaces, Bar-Cohen, and Rohsenow [22] for two vertical surfaces, not for ducts. Therefore, compression with [10] and [15] whose channel size is more than ten times than the current test trig. Figures 8a and 8b show the Nu(s) and Nu(H) against Ra^*s/H. The current results show good presentation for both cases (R^2 above 0.9). However, results from [10] and [15] show only an acceptable presentation for the Nu(s) (R^2 above 0.6). The errors can be attributed to the nature of their experiment and the amount of data they handled. The discrepancy between the current and their data can be justified to the nature of flow, heat inputs, geometry, or aspect ratio of the three works. However, both sides in Figure 9c present very good correlation factors (R^2 above 0.93) and close curve slope, but their data are not close to the current results. This can be attributed to the same factor mentioned earlier. For example, LaPica etal [15] believed that they dealt with a turbulent flow as they observed a fluctuation of temperature in a range of about ±5°C at the exit at high Ra^* (over 7 x 1012). Finally, Figure 9d shows a very good presentation of current and those from [10] and [15] - R^2 above 0.95. This can be summarized by curve-fitting equations as follows:

$\dot{m} \propto (s/H)^{0.66}$ (Current Results)

$\dot{m} \propto (s/H)^{0.71}$ (Ref. 10 Results)

$\dot{m} \propto (s/H)^{0.4}$ (Ref. 15 Results).

Based on s/H, no obvious trend can be attributed to determine values of exponents, but it could be based on other factors such as geometry or heat inputs and may be due to minor causes like surface roughness and pressure losses. . Therefore, it is recommended to study the problem further and clarify the issue.

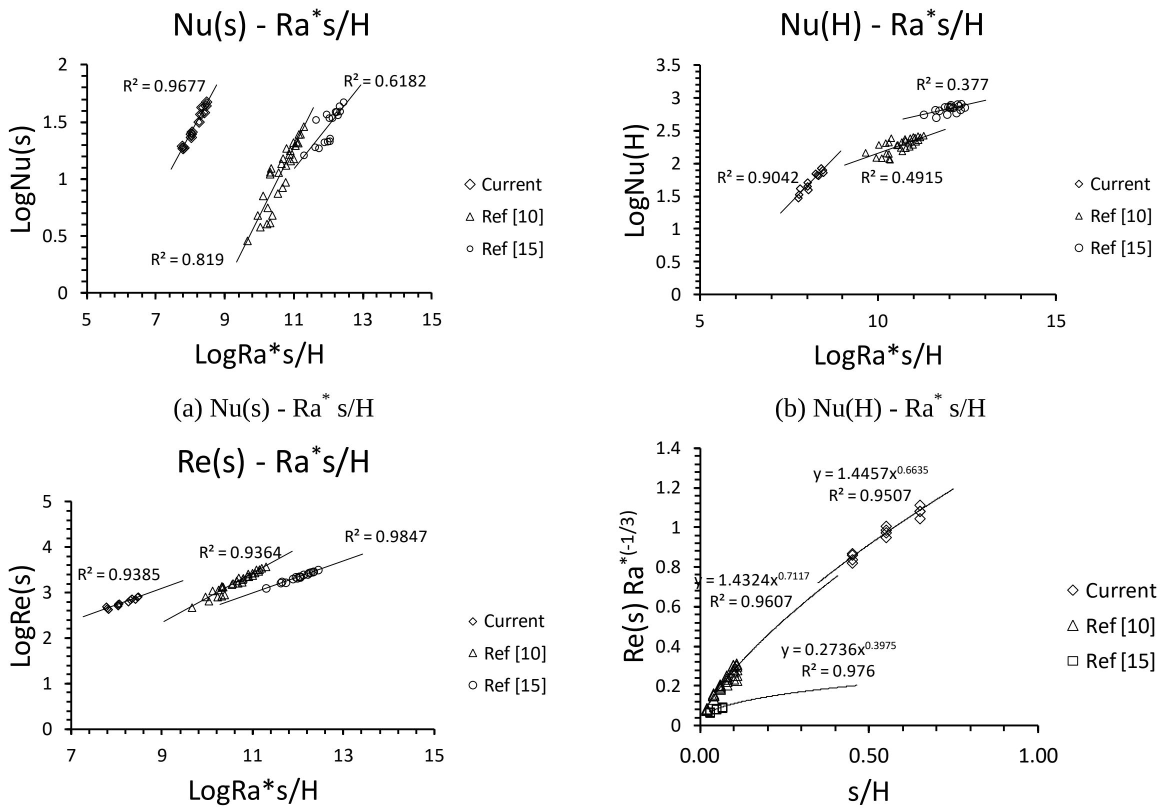

(a) Nu(s) - Ra^* s/H

(b) Nu(H) - Ra^* s/H

(c) Re(s) - Ra^* s/H

(d) Re(s) $Ra^{*(-1/3)}$ - s/H

Figure 9: Dimensionless Numbers Compressions**.**

8. Conclusion:

Airflow induced by bouncy-driven convection heat transfer in a vertical channel (duct) has been extensively studied in this work under UHF heating mode. Two variables were introduced (Q_{in} and s/H) to investigate their effects on the thermal and the hydraulic performance of the airflow inside the channel. The main outcomes of the current study are summarized as follows:

- Various dimensionless correlations in regard to mass and heat transfer were presented in terms of Nu and Re(s). According to equations 10 to 16;

$$\mathrm{Nu(s)} = 0.0008\,(\mathrm{Ra}^*\ \ \mathrm{s/H})^{0.563}$$
$$\mathrm{Nu(H)} = 0.0018\,(\mathrm{Ra}^*\ \ \mathrm{s/H})^{0.551}$$
$$\mathrm{Re(s)} = 0.7602\,(\mathrm{Ra}^*\ \mathrm{s/H})^{0.357}$$

Accordingly,

$$\mathrm{Nu} \propto (\mathrm{Ra}^*\ \mathrm{s/H})^{\approx 0.5}$$

and,

$$\mathrm{Re(s)} \propto (\mathrm{Ra}^*\ \mathrm{s/H})^{\approx 0.35}$$

- The lumped-parameter model demonstrates a good representation and shows data the dependency of flow rate on the depth-to-height aspect ratio (s/H) is close to 0.66:

$$\dot{m} \propto (\mathrm{s/H})^{0.66}$$

Further Work:

The effect of the aspect ratio and the variations of the heat input on the airflow were studied in the current project. However, in order to complete the picture, it is suggested that the effect of the variations of inclination angle as well as the variation of the channel heights is recommended to be studied. In addition, developing a numerical model would reduce the time-consuming and physical effort, using, for example, Fluent or Pheonics CFD Code. It is important to state and emphasize that these studies of the airflow induced by natural convection, particularly under the UHF heating mode, have not been completely covered. Therefore, it is recommended to study the classification of the flow regime under the UHF heating mode for these applications since no more studies have been done with regard except the work of Vliet and Ross [4] and Bar-Cohen and Rohsenow [22], who presented correlations in laminar and turbulent airflow regimes, but they are applied to ducts.

Acknowledgment
I would like to thank all who offer support, consultation and assistance to complete this work.

Nomenclature

a, b, c	Regression coefficients (see Equation 7).
A_C	Cross section area of the channel (s x w) m^2.
A_P	Hot plate Area (0.01m^2).
Gr(H)	Grashof number based on H ($Gr(H) = \frac{g\,\beta\,\Delta T\,H^3}{\nu^2}$).
g	Acceleration due to gravity (= 9.81 m/s^2).
H	Convective heat transfer (W/m^{2}K).
H	Channel height = 1m.
k	Thermal conductivity of air (W/m.K).
k'	Regression parameter in Equation 1: inverse of time constant (1/s).
ṁ	Airflow rate (kg/s).
Pa	Ambaint Pressure.
Pr	Prandtl number.
q_c	Convective heat to airstream (W/m^2)
q_{in}	Heat input (W/m^2).
Ra	Rayleigh number.
Re(s)	Reynolds number based on channel depth.
s	Channel depth (m).
t	Time (s).
T	Temperature (°C).
T_i	Inlet mean temperature (°C).
T_a	Ambient Temperature (°C).
T_m	Mean temperature of air in the channel = [(T_i+T_o)/2] (°C).
T_o	Outlet mean temperature (°C).
T_p	Hot plate mean temperature (°C).
ū	Air bulk velocity (m/s).
w	Channel width = 0.1m.
y	Regression parameter in Equation 1.
y_o	Final (asymptotic) value of y.

Greek symbols:

β	Expansion coefficient (1/K).
ρ_i	Density (kg/m^3).
ν	Kinematic viscosity (m^2/s).

References:

[1] Churchill, S. W., and Chu, H. H. S. (1975). Correlating equations for laminar and turbulent free convection from a vertical plate. International Journal of Heat and Mass Transfer, 18 (11).
[2] Sparrow, E. M., and Gregg, J. L. (1956). Laminar free convection from a vertical plate with uniform surface heat flux. Transactions of the ASME, 78, 435–440.
[3] Sparrow, E. M., and Gregg, J. L. (1958). Similar solutions for free convection from a nonisothermal vertical plate. Transactions of the ASME, 80, 379–386.
[4] Vliet, G. C., and Ross, D. C. (1975). Turbulent natural convection on upward and downward facing inclined constant heat flux surfaces. Journal of Heat Transfer, 97, 549–555.
[5] Beckman, W. A., Blair, N., and Duffie, J. A. (2020). Solar engineering of thermal processes, photovoltaics and wind. John Wiley and Sons.
[6] Norton, B., Hobday, R. A., and Lo, S. N. G. (1992). Thermosyphoning air panels. In K. W. Böer (Ed.), Advances in Solar Energy: An Annual Review of Research and Development (Vol. 7, pp. 495–571). American Solar Energy Society.
[7] Akbari, H., and Borgers, T. R. (1979). Free convective laminar flow within the Trombe wall channel. Solar Energy, 22(2).
[8] Borgers, T. R., and Akbari, H. (1984). Free convective turbulent flow within the Trombe wall channel. Solar Energy, 33(3–4).
[9] Laatar, A. H., Kennich, S., Balti, J., and Badi, N. (2019). Natural convection in inclined channel for air cooling of photovoltaic panels. Experimental and Theoretical Nanotechnology.
[10] Burek, S. A. M., and Habeb, A. (2007). Air flow and thermal efficiency characteristics in solar chimneys and Trombe walls. Energy and Buildings, 39(2).
[11] Bouchair, A. (1994). Solar chimney for promoting cooling ventilation in southern Algeria. Building Services Engineering Research and Technology, 15(2).

[12] Cherif, Y., Sassine, E., Lassue, S., and Zalewski, L. (2019). Experimental and numerical natural convection in an asymmetrically heated double vertical facade. International Journal of Thermal Sciences, 152.
[13] Dong, C., Lu, G., Chen, R., Zhang, K., Liu, C., Tian, W., Qiu, S., and Su, G. H. (2023). Experimental study on turbulent natural convection of air between the open-ended parallel plates with one-side heating. Annals of Nuclear Energy, 181.
[14] Kim, K. M., Nguyen, D. H., Shim, G. H., Jerng, D. W., and Ahn, H. S. (2020). Experimental study of turbulent air natural convection in open-ended vertical parallel plates under asymmetric heating conditions. International Journal of Heat and Mass Transfer, 159.
[15] La Pica, A., Rodonò, G., and Volpes, R. (1993). An experimental investigation on natural convection of air in a vertical channel. International Journal of Heat and Mass Transfer, 36(3).
[16] Miyamoto, M., Katoh, Y., Kurima, J., and Sasaki, H. (1986). Turbulent free convection heat transfer from vertical parallel plates. In Proceedings of the International Heat Transfer Conference (Vol. 4).
[17] Sandberg, M., and Moshfegh, B. (2002). Buoyancy-induced air flow in photovoltaic facades: Effect of geometry of the air gap and location of solar cell modules. Building and Environment, 37(3).
[18] Elenbaas, W. (1942). Heat dissipation of parallel plates by free convection. Physica, 9(1).
[19] Azevedo, L. F. A., and Sparrow, E. M. (1985). Natural convection in open-ended inclined channels. Journal of Heat Transfer, 107(4).
[20] Khoualdi, T., Rouabah, M. S., Bouraoui, M., Abidi-Saadb, A., and Polidori, G. (2018). Free convection heat transfer in an inclined channel asymmetrically heated in laminar regime. International Journal of Heat and Technology, 36(3).
[21] Onur, N., and Aktaş, M. K. (1998). An experimental study on the effect of opposing wall on natural convection along an inclined hot plate facing downward. International Communications in Heat and Mass Transfer, 25(3).
[22] Bar-Cohen, A., and Rohsenow, W. M. (1984). Thermally optimum spacing of vertical natural convection cooled, parallel plates. Journal of Heat Transfer, 106, 116–123.
[23] Baskaya, S., Aktas, M. K., and Onur, N. (1999). Numerical simulation of the effects of plate separation and inclination on heat transfer in buoyancy driven open channels. Heat and Mass Transfer, 35(4), 273–280.
[24] Khoualdi, T., Rouabah, M. S., Bouraoui, M., Abidi-Saadb, A., and Polidori, G. (2018). Free convection heat transfer in an inclined channel asymmetrically heated in laminar regime. International Journal of Heat and Technology, 36(3), 1140–1147.
[25] Habib, M. A., Said, S. A. M., Ahmed, S. A., and Asghar, A. (2002). Velocity characteristics of turbulent natural convection in symmetrically and asymmetrically heated vertical channels. Experimental Thermal and Fluid Science, 26(1).
[26] Qasem, N. A. A., Imteyaz, B., Ben-Mansour, R., and Habib, M. A. (2017). Effect of radiation heat transfer on naturally driven flow through parallel-plate vertical channel. Arabian Journal for Science and Engineering, 42, 1817–1829.
[27] Habeb, A. (2016). Airflow and heat transfer by natural convection in small-scale vertical channel. 1st International Conference on Chemical, Petroleum, and Gas Engineering (ICCPG), Al-Mergib University, Libya. https://elmergib.edu.ly/iccpge/iccpgePapers/261.pdf
[28] Incropera, F. (2016). Fundamentals of heat and mass transfer. John Wiley and Sons.
[29] Yilmaz, T. (1997). An experimental and numerical investigation of laminar and turbulent natural convection in vertical parallel-plate channel (PhD thesis). Department of Mechanical Engineering, University of Strathclyde.
[30] Yilmaz, T., and Fraser, S. M. (2007). Turbulent natural convection in a vertical parallel-plate channel with asymmetric heating. International Journal of Heat and Mass Transfer, 50, 2612–2623.
[31] Yilmaz, T., and Gilchrist, A. (2007). Temperature and velocity field characteristics of turbulent natural convection in a vertical parallel-plate channel with asymmetric heating. Heat and Mass Transfer, 43, 707–719.